Hydroxyapatite microparticles as feed-back active reservoirs of corrosion inhibitors

D. Snihirova[1], S. V. Lamaka[1], M. Taryba[1], A. N. Salak[2], S. Kallip[2], M. L. Zheludkevich[2], M.G.S. Ferreira[1,2], M.F.Montemor[1]*

[1] ICEMS, Instituto Superior Tecnico, UTL, Av. Rovisco Pais, 1049-001 Lisbon, Portugal

[2] CICECO, Dep.Ceramics and Glass Eng., University of Aveiro, 3810-193, Aveiro, Portugal

[*] sviatlana.lamaka@ist.utl.pt

Supporting information

HPLC. High performance liquid chromatography was used to determine the loading capacity of HAP for 8-HQ and Sal and measure release at different pH. A PerkinElmer 200LC pump, an UV-detector and Grace Smart RP-18 (4.6×250mm, 5μm) column were used. 20μl of the sample was injected into the column using a sample loop. The chromatographic conditions for determination of 8-hydroxyquinoline were optimized as follows: acetonitrile-water (65:35 v/v) pH = 3.05 was used as a mobile phase; flow rate was 0.8ml/min; UV signal was recorded at 240nm; retention time was 4.23 min. The optimized chromatographic conditions for salicylaldoxime quantification: mobile phase was a mixture of methanol-water-5% phosphoric acid (40:60:4 v/v); flow rate was 1.1ml/min; UV detection was carried out at 301nm, retention time was 8.14min. TotalChrom 6.3 software was used for data processing.

Preparation of pH-selective microelectrodes. The pH selective microelectrodes were prepared from single-barreled, standard-wall (330 micron) borosilicate glass capillaries with an outer-diameter of 1.5 mm. A P-97 Flaming/Brown Micropipette Puller (Sutter Instruments) was used to shape the cone tip. The diameter of the apex of the tip was 2.0 ± 0.5 μm. Before use, the inner surface of the capillaries was silanized by injecting 200 μL of N,N-dimethyltrimethylsilylamine in a glass preparation chamber at 200°C. The silanized microelectrodes were back-filled with the inner filling solution and tip-filled with a selective ionophore-based oil-like membrane. The ion-selective membrane was composed of 6 wt% 4-nonadecylpyridine, 12 mol% potassium tetrakis(4-chlorophenyl)borate and membrane solvent 2-nitrophenyloctyl ether. All reagents for the pH-

selective membrane were Selectophore grade products from Fluka. The column length of the membrane was about 60 - 70 μm. A chlorinated silver wire was inserted into the inner filling solution as the internal reference electrode. The inner filling solution contained a buffer solution composed of 0.01M KH_2PO_4 and 0.1M KCl. The microelectrodes were calibrated using commercially available (Fluka) pH buffers. A homemade Ag/AgCl/0.1M KCl, 0.01M KH_2PO_4 electrode with an inner solution stabilized by 3% agar-agar was used as external reference electrode. The microelectrodes demonstrated a stable and reproducible potential in the pH range 2 to 10 with a linear response slope of -54.8 ± 0.7 mV/pH.

FTIR. Fourier transform infrared spectroscopy measurements were performed using a Mattson Galaxy 3020 Spectrophotometer. The samples were prepared by mixing ~2 mg of HAP with ~300 mg of spectroscopic-grade KBr (Merck) and pressing the mixture into a disk. The infrared spectrum, Fig.S1, was recorded in transmittance mode between 4000 and 300 cm^{-1} with a resolution of 4 cm^{-1}.

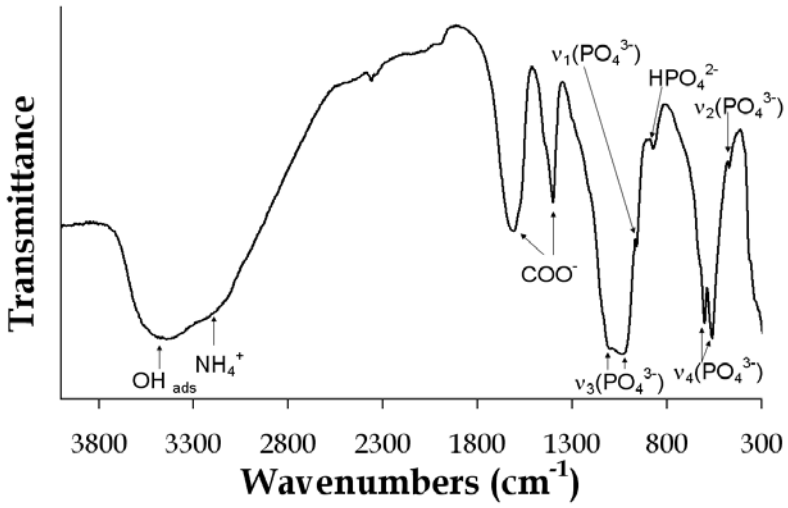

Figure S1. FTIR spectrum of the hydroxyapatite microparticles.

Two strong bonds, at 1405 and 1595 cm^{-1}, assigned to citrate carboxylate groups COO− (asymmetric and symmetric stretching, respectively) were observed. The typical FTIR spectrum also shows the main vibration bonds for the hydroxyapatite PO_4^{3-} groups at 1087, 1040, 962, 601, 571 and 474 cm^{-1}. The first peak, at 1087 cm^{-1}, arises from a triple degenerate asymmetric stretching mode vibration, υ_3. The other component of this degenerate vibration, $\upsilon 3$, of the P–O bond appears at 1040 cm^{-1}. The peak at 962 cm^{-1} is assigned to a nondegenerate symmetric stretching mode, υ_1. The peaks at 601 and 571 cm^{-1} are assigned to a doubly degenerate bending

mode, υ_4, of the O–P–O bond. The weak peak at 474 cm^{-1} is a component of the degenerate bending mode, υ_2. The broad band at 3400 cm^{-1} can be assigned to adsorbed water molecules. In addition, a broad band detected at 3200 cm^{-1} accounts for the presence of ammonium ions, NH_4^+ [1S-3S].

XRD. Phase analysis of the precipitated powders of hydroxyapatite and hydroxyapatite-derived compositions was performed by X-ray diffraction using a Rigaku D/MAX-B diffractometer (Cu Kα radiation, tube power 40 kV, 30 mA; graphite monochromator, receiving slit of 0.15 mm). The XRD data was collected over an angular range of $10<2\theta<80^o$ with 0.02º steps and exposition of 5 s/step. For the crystal structure characterization, the detailed data was recorded using a Philips X'Pert MPD diffractometer (Ni-filtered Cu Kα radiation, tube power 40 kV, 50 mA; X'celerator detector, and the exposition corresponded to 14 s per step of 0.02º over the same 2θ range) at room-temperature. The obtained data was refined by the Rietveld method using the FULLPROF suite [4S].

XRD analysis was performed in order to assess the changes in the crystalline structure of the hydroxyapatite after doping with the different inhibiting compounds. Blank HAP, as well as the hydroxyapatite powders treated with salicylaldoxime and lanthanum nitrate (HAP-Sal and HAP-La(III)) were characterized. The diffraction patterns of HAP and HAP-Sal show that the treatment with salicylaldoxime does not change the crystalline structure of hydroxyapatite, Fig. S2a. At the same time, small shifts in the diffraction peaks were observed suggesting differences in the values of the lattice parameters (see inset in Fig. S2a). Treatment with lanthanum results in decomposition of the hydroxyapatite phase. HAP-La(III) presents a mixture of calcium- and lanthanum-based phases, where calcium phosphate oxide $Ca_{10}(PO_4)_6O$ and lanthanum phosphate $LaPO_4$ are the dominant compounds (Fig. S2a).

The characteristic reflections in the XRD patterns of both HAP and HAP-Sal are indicative of the monoclinic symmetry [5S, 6S]. Indeed, the crystal structure of these compositions was successfully refined using the monoclinic $P2_1/b$ space group. Fig. S2b shows the results of the refinement in the case of HAP-Sal. The obtained values of the structure parameters are listed in Table S1. An attempt to refine the XRD data using the hexagonal $P6_3/m$ space group was made, as this symmetry was previously attributed to the $[Ca_5(PO_4)_3(OH)]_2$ hydroxyapatite [7S] and to other related hydroxyapatites with a Ca/P molar ratio different from 5:3 [8S]. However, the monoclinic symmetry (space group $P2_1/b$) provided a better fit in respect to both the description of the diffraction profiles and values of the reliability factors.

The lattice parameters of HAP (Table S1) were compared with the respective data available from literature. One will notice some spread in the values of the parameters reported by different authors

[5S, 6S, 9S]. In this study, the value of parameter *a* is larger and that of parameter *b* is smaller than those typically observed for $[Ca_5(PO_4)_3(OH)]_2$ hydroxyapatite [5S, 6S]. The ratios between the values of *a*, *b* and *c* for HAP as well as the magnitude of the angle γ suggest that this composition is characterized by a higher degree of monoclinic distortion than other hydroxyapatites previously reported.

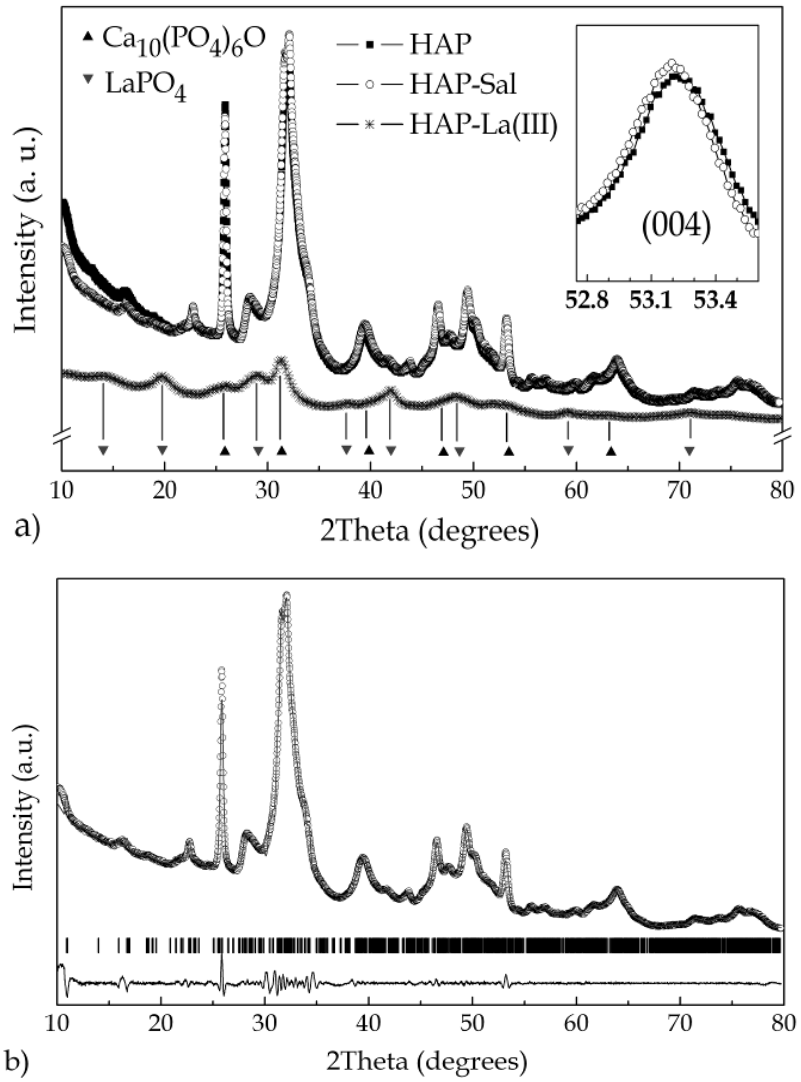

Figure S2. a) XRD patterns of HAP, HAP-Sal, and HAP-La(III) at room temperature. The main phases identified in the HAP-La(III) powder are also indicated. Inset: the diffractograms of HAP and HAP-Sal at the region of the (004) reflections. b) Observed (○), calculated (solid line), and difference (below) profiles of the XRD data on HAP-Sal refined in space group $P2_1/b$. Vertical bars represent the calculated peak positions.

Table S1. The representative crystal structure parameters obtained from the refinement of the room-temperature XRD data for HAP and HAP-Sal.

composition	*a* (Å)	*b* (Å)	*c* (Å)	γ (°)
HAP	9.4426(9)	18.4788(19)	6.8815(5)	118.711(4)
HAP-Sal	9.4545(9)	18.4895(18)	6.8862(5)	118.714(4)

The modelling of ionic equilibria relative to Ca^{2+} (Fig. S3) predicts initiation of HAP dissolution at pH 8, that is in good agreement with the release trend of organic inhibitors, see Fig 6.

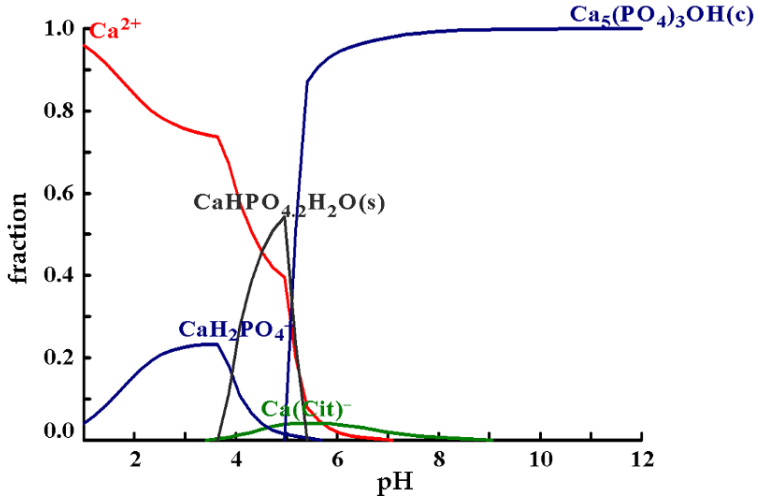

Figure S3. Fraction of all Ca^{2+} containing ions depending on pH in solution that contains citrate and phosphate ions at the following concentrations: [Ca^{2+}]= 0.1M, [PO^{3-}_4]= 0.06M, [Cit^{3+}]= 0.005M. The diagram was made using Hydra/Medusa software [10S].

References:

1S. Houwena J. A.M.; Cresseya G.; Cresseyb B. A.; Valsami-Jonesa E. *J. Cryst. Growth.* **2003**, 249, 572-583.

2S. Mitsionis A. I.; Vaimakis T. C.; Trapalis C. C. *J. Ceram Inter.* **2010**, 36, 623-634.

3S. Elliott J.C. *Structure and Chemistry of the Apatites and Other Calcium Orthophosphates*, Elsevier: London, **1994**; Vol 18, p. 111-116.

4S. Rodriguez-Carvajal J. *Phys. B: Condensed Matter* **1993**, 192, 55-69.

5S. Ikoma T.; Yamazaki A.; Nakamura S.; Akao M. *J. Solid State Chem*. **1999**, 144, 272-276.

6S. Suetsugu Y.; Tanaka J. *J. Mater. Sci.: Materials in Medicine* **2002**, 13, 767-772.

7S. Pritzkow W.; Rentsch H. *Crystal Research and Tech.* **1985**, 20, 957-960.

8S. Wilson R.M.; Elliot J.C.; Dowker S.E.P. *J. Solid State Chem.* **2003**, 174, 132-140.

9S. Elliott J. C.; Mackie P.E.; Young R.A. *Science* **1973**, 180, 1055-1057.

10S. Puigdomenech, I. *Program MEDUSA (Make equilibrium diagrams using sophisticated algorithms)* **1999** Royal Institute of Technology, Stockholm